

PAPER

## A Monte-Carlo study to assess the effect of 1.5 T magnetic fields on the overall robustness of pencil-beam scanning proton radiotherapy plans for prostate cancer

To cite this article: Christopher Kurz *et al* 2017 *Phys. Med. Biol.* **62** 8470

View the [article online](#) for updates and enhancements.

### You may also like

- [Impact source identification in finite isotropic plates using a time-reversal method: theoretical study](#)  
Chunlin Chen and Fuh-Gwo Yuan
- [Performance of Geogrid Reinforced Concrete Slabs under Drop Weight Impact Loading](#)  
T J Vijay, K Rajesh Kumar, R Vandhiyan et al.
- [Study on Dynamic Response Characteristics of Bird Impact Glass Fiber Laminate](#)  
Yang Liu, Jia Qu, Xiaojun Yan et al.

# A Monte-Carlo study to assess the effect of 1.5 T magnetic fields on the overall robustness of pencil-beam scanning proton radiotherapy plans for prostate cancer

Christopher Kurz<sup>1</sup>, Guillaume Landry<sup>2</sup>, Andreas F Resch<sup>2,3</sup>,  
George Dedes<sup>2</sup>, Florian Kamp<sup>4</sup>, Ute Ganswindt<sup>4</sup>,  
Claus Belka<sup>4,5</sup>, Bas W Raaymakers<sup>1</sup> and Katia Parodi<sup>2</sup>

<sup>1</sup> Department of Radiotherapy, University Medical Center Utrecht, Utrecht, Netherlands

<sup>2</sup> Faculty of Physics, Department of Medical Physics,  
Ludwig-Maximilians-Universität München, Munich, Germany

<sup>3</sup> Department of Radiotherapy, Christian Doppler Laboratory for Medical Radiation Research for Radiation Oncology, Medical University of Vienna/AKH Wien, Vienna, Austria

<sup>4</sup> Department of Radiation Oncology, University Hospital, LMU Munich, Munich, Germany

<sup>5</sup> German Cancer Consortium (DKTK), Munich, Germany

E-mail: [c.kurz@umcutrecht.nl](mailto:c.kurz@umcutrecht.nl)

Received 30 May 2017, revised 12 September 2017

Accepted for publication 20 September 2017

Published 19 October 2017



## Abstract

Combining magnetic-resonance imaging (MRI) and proton therapy (PT) using pencil-beam scanning (PBS) may improve image-guided radiotherapy. We aimed at assessing the impact of a magnetic field on PBS-PT plan quality and robustness. Specifically, the robustness against anatomical changes and positioning errors in an MRI-guided scenario with a 30 cm radius 1.5 T magnetic field was studied for prostate PT.

Five prostate cancer patients with three consecutive CT images (*CT1-3*) were considered. Single-field uniform dose PBS-PT plans were generated on the segmented *CT1* with Monte-Carlo-based treatment planning software for inverse optimization. Plans were optimized at 90° gantry angle without B-field (*no B*), with ±1.5 T B-field (*B* and *minus B*), as well as at 81° gantry angle and +1.5 T (*B G81*). Plans were re-calculated on aligned *CT2* and *CT3* to study the impact of anatomical changes. Dose distributions were compared in terms of changes in DVH parameters, proton range and gamma-index

pass-rates. To assess the impact of positioning errors, DVH parameters were compared for  $\pm 5\text{ mm}$  CT1 patient shifts in anterior–posterior (AP) and left–right (LR) direction.

Proton beam deflection considerably reduced robustness against inter-fractional changes for the *B* scenario. Range agreement, gamma-index pass-rates and PTV V95% were significantly lower compared to *no B*. Improved robustness was obtained for *minus B* and *B G8I*, the latter showing only minor differences to *no B*. The magnetic field introduced slight dosimetric changes under LR shifts. The impact of AP shifts was considerably larger, and equivalent for scenarios with and without B-field.

Results suggest that robustness equivalent to PT without magnetic field can be achieved by adaptation of the treatment parameters, such as B-field orientation (*minus B*) with respect to the patient and/or gantry angle (*B G8I*). MRI-guided PT for prostate cancer might thus be implemented without compromising robustness compared to state-of-the-art CT-guided PT.

**Keywords:** intensity-modulated proton therapy, magnetic resonance imaging, image-guided radiotherapy, prostate cancer

(Some figures may appear in colour only in the online journal)

## 1. Introduction

External beam radiotherapy has seen considerable progress with the clinical implementation of highly conformal irradiation techniques, such as intensity-modulated photon (IMRT) and proton (IMPT) therapy, as well as *in situ* image-guidance (Jaffray 2012, Mendenhall *et al* 2014), which is near-ubiquitous in IMRT. While IMPT using pencil-beam scanning (PBS) (Durante and Loeffler 2010) is also becoming widely implemented, volumetric image-guidance in proton therapy (PT) is still in its infancy (Engelsman *et al* 2013). Only recently have proton facilities been equipped with in-room x-ray computed-tomography (CT) scanners (Stuetzer *et al* 2016) or dedicated cone-beam CT (CBCT) imaging systems (Rit *et al* 2016). Although these devices allow daily assessment of patient position and anatomy or dose calculation (Kurz *et al* 2015, Kurz *et al* 2016, Veiga *et al* 2016), their soft tissue contrast is generally poor. In conventional photon radiotherapy this led to the development of combined magnetic-resonance imaging (MRI) radiotherapy devices (Fallone 2014, Keall *et al* 2014, Lagendijk *et al* 2014a, 2014b, Mutic and Dempsey 2014). Beyond improved target visualization (Rasch *et al* 1999, Noel *et al* 2015) and pre-treatment plan adaptation (Acharya *et al* 2016), MRI-guided radiotherapy promises intra-fractional imaging (Glitzner *et al* 2015) and real-time adaptation (Kontaxis *et al* 2015) without additional dose burden. Consequently, there is growing interest in combining PBS-PT with MRI.

Up to now only few studies on MRI-guided PT have been conducted. Most deal with simplified phantom scenarios and beam set-ups (Raaymakers *et al* 2008, Wolf and Bortfeld 2012, Fuchs *et al* 2017, Schellhammer and Hoffmann 2017). In a more clinical study, Moteabbed *et al* demonstrated the dosimetric feasibility of passively scattered proton treatment in magnetic fields by manually modifying the initial beam angle and iso-center position (Moteabbed *et al* 2014). The feasibility of inverse PBS-PT plan optimization in a B-field was shown by Hartman *et al* (2015), considering, however, relatively small lesions (<11 cc) and a simplified patient representation (outer contour filled with water).

One clinical indication expected to benefit from MRI-guided PBS-PT is prostate cancer. Here, PBS-PT promises highly conformal dose shaping at reduced integral dose (Trofimov *et al* 2007), while MRI-guidance enables improved target visualization (Villeirs *et al* 2005, Lutgendorf-Caucig *et al* 2011) and alignment without fiducials, as well as, potentially in the future, monitoring of intra-fractional motion (e.g. prostate drifts, changes in rectum and bladder filling (Padhani *et al* 1999, Kotte *et al* 2007, Beltran *et al* 2008)) and online adaptive PBS-PT.

However, even though MRI-guidance suggests the implementation of adaptive treatment strategies in the future, the robustness of the applied treatment might nonetheless be clinically important, particularly when considering the short time-scale of anatomical changes for prostate cancer patients. An MRI-guided plan optimized prior to delivery should be as robust to anatomical changes, such as prostate and bowel-movement, as a plan delivered in the absence of a magnetic field. Thus, the goal of this contribution was to investigate for the first time whether the robustness of PBS-PT against anatomical changes and positioning errors is affected by the presence of a magnetic field. To this aim, a dedicated Monte-Carlo (MC)-based research treatment planning tool was adapted and utilized for inverse PBS-PT optimization in a magnetic field. Repeated daily CT data of prostate cancer patients were used to assess treatment robustness. Different field orientations and gantry angles were studied to demonstrate how an improved robustness of MRI-guided PBS-PT might be attained.

## 2. Material and methods

### 2.1. Patient cohort

Five prostate cancer patients (Pat1-5) originally treated with IMRT were included in this study. For each patient three CTs (*CT1-3*) were acquired on consecutive days with a Toshiba Aquilion LB scanner (Toshiba Medical Systems, the Netherlands) and contoured by a single physician. *CT2/3* were rigidly registered to *CT1* focusing on bony anatomy in close vicinity to the PTV, since no markers were implanted. No bladder or rectal filling protocol was applied, such that the data represent an extreme scenario in terms of anatomical changes. Based on the prostate motion observed on the three available CT data-sets of each patient, an isotropic clinical target volume (CTV) to planning target volume (PTV) margin of 10 mm was applied during the original IMRT treatment. For the PBS-PT treatment scenario investigated in this work, the lateral margin due to inter-fractional motion and positioning uncertainties was assumed to be similar. For the margin along the beam axis, i.e. in left-right (LR) direction, it should be noted that LR patient shifts do not strongly impact the proton range and that prostate motion was typically less pronounced in this direction. Estimating, however, a positioning uncertainty of 3 mm and a range margin of 1.5 mm plus 3% of the proton range (Paganetti 2012) (approximately 20 cm for this patient cohort) a similar margin was estimated in beam direction, and thus the original isotropic 10 mm margin was kept in this study.

### 2.2. Treatment planning

For inverse PBS-PT treatment planning in magnetic fields, the capabilities of an in-house MC-based treatment planning tool were extended. The research tool models a generic PBS system and is not based on a clinical beam model. It uses a particle therapy extension of CERR for treatment planning (Matlab 2014a, (Deasy *et al* 2003, Schell and Wilkens 2010)), coupled with Geant4 (version 10.02, (Agostinelli *et al* 2003)) MC dose calculations, and follows the

approach described in Resch *et al* (2017). First, lateral positions and energies of pencil-beams with their Bragg-peak located in the PTV are determined in CERR. Lateral pencil-beam spacing was fixed to 4 mm, longitudinal spacing to 3 mm. Positions and energies were then exported to Geant4 and the dose distribution of each pencil-beam calculated on *CT1* using the CT voxel grid of 1.074 mm × 1.074 mm × 3 mm and 10<sup>5</sup> protons. The QGSP\_BIC\_HP physics list was employed. A generic pencil-beam width of 5 mm standard deviation and an initial energy spread of 0.5% were assumed (Parodi *et al* 2012) and beam divergence neglected. The CT was converted into elemental composition and density following the approach of Schneider *et al* (2000), calibrated for the specific CT scanner. The MC-calculated dose distributions of all pencil-beams were re-imported to CERR and used for optimizing the pencil-beam weights to derive the final PBS-PT plan. For modelling the presence of an MRI magnetic field, an infinite homogeneous cylindrical 1.5 T B-field with a radius of 30 cm (midpoint aligned to CT center) was introduced during pencil-beam dose calculation. The field strength of 1.5 T was chosen as the highest field strength in current designs of combined conventional MRI-radiotherapy devices (Lagendijk *et al* 2014b). The magnetic field was aligned with the superior–inferior (SI) direction of the patient and perpendicular to the proton beam. In order to account for the magnetic deflection of the pencil-beams in anterior–posterior (AP) direction, initial pencil-beam generation in CERR used a virtual, expanded PTV, displaced in AP by approximately 4 cm, which corresponds to a beam iso-center shift by the same distance. Note that the size of this shift is specific for the modeled B-field geometry and strength, in combination with the location of the target volume within the patient and the proton energy of about 150–200 MeV required to reach it.

Single-field uniform dose (SFUD) plans were generated for all five patients on *CT1* at a gantry angle of 90° (on the International Electrotechnical Commission scale) without B-field (referred to as *no B*, used as reference), with +1.5 T and −1.5 T B-field (*B* and *minus B*), as well as at a gantry angle of 81° with +1.5 T B-field (*B G81*). The latter scenario aimed at correcting for the proton beam deflection in the sense of reproducing a similar beam entrance position and trajectory within the patient as for the *no B* reference. Similar to the iso-center shift, the exact size of the applied gantry angle correction, in this case 9°, is specific to the investigated scenario of prostate cancer patients where a certain proton beam energy is required to reach the target, as well as to the chosen shape and strength of the magnetic field. The angle of 81° was selected following manual tuning of the gantry angle in the range from 90° to 78° for exemplary patient cases. The gantry angle showing the smallest deviation of the proton beam path within the patient when compared to the *no B* scenario (i.e. with the beam most parallel to *no B*) was then chosen. All treatment plans were scaled to a PTV median dose of 74 Gy. Optimization aimed at CTV  $V_{95\%}$  of 100%, PTV  $V_{95\%}$  above 98% and PTV  $D_{2\%}$  below 76 Gy. For the OARs, following the QUANTEC report (Marks *et al* 2010), planning aimed at rectum  $V_{50\text{ Gy}} < 50\%$ ,  $V_{60\text{ Gy}} < 35\%$ ,  $V_{65\text{ Gy}} < 25\%$  and  $V_{70\text{ Gy}} < 20\%$ , as well as bladder  $V_{65\text{ Gy}} < 50\%$  and  $V_{70\text{ Gy}} < 35\%$ .

### 2.3. Data analysis

To assess robustness against anatomical changes, the plans of *no B*, *B*, *minus B* and *B G81* scenarios were re-calculated on registered *CT2* and *CT3*, using Geant4. Dosimetric differences with respect to *CT1* were evaluated based on CTV  $D_{98\%}$  and  $V_{95\%}$ , PTV  $D_{2\%}$  and  $V_{95\%}$ , rectum  $V_{50/60/65/70\text{ Gy}}$ , as well as bladder  $V_{65/70\text{ Gy}}$ , using the CT-specific contours. Dose distributions on *CT2/3* were also compared to those on *CT1* by means of a (2%, 2 mm) global gamma-criterion, considering voxels above 60% of 74 Gy. Proton range, defined at the 80%

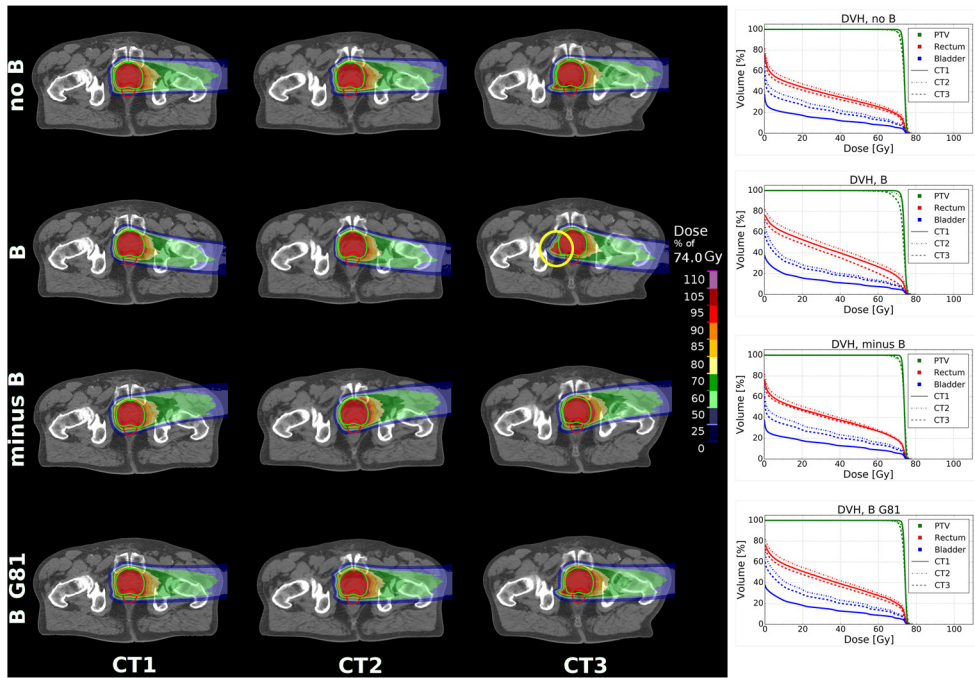


**Figure 1.** Dose distributions and DVHs for Pat1. The PTV and rectum are depicted in green and red, respectively. Dose distributions optimized on CT1 (left column) and re-calculated on CT2/3 (second and third column) are shown for the *no B* (top row), *B* (second row), *minus B* (third row) and *B G81* scenarios (bottom row). A substantial overshoot on CT3 for the *B* case is indicated by the yellow circle.

distal dose fall-off, on *CT2/3* and *CT1* was compared in beam's eye view (BEV), assuming a gantry angle of 90° (also for *B G81*). The pass-rate of BEV profiles with a range agreement better than 3 mm was determined, considering BEV dose profiles with a maximum of at least 80% of 74 Gy.

For investigating the robustness against positioning errors, AP and LR shifts of ±5 mm (Trofimov *et al* 2011) of *CT1* were introduced and the dose re-calculated using Geant4. Dosimetric changes with respect to the reference without shift of *CT1* were evaluated by means of the same dose–volume histogram (DVH) parameters mentioned above.

Statistically significant differences between *no B* reference and *B*, *minus B* or *B G81* scenario in all evaluated parameters were determined using a paired Wilcoxon signed-rank test at a significance level of  $p = 0.05$ .

### 3. Results

#### 3.1. Robustness against anatomical changes

Figure 1 shows the dose optimized on *CT1* (left column) for *no B*, *B*, *minus B* and *B G81* scenarios, as well as the re-calculations on *CT2* and *CT3* (second and third column) together with the corresponding DVHs (right column) for exemplary patient Pat1. The 30 cm radius 1.5 T magnetic field introduces a noticeable curvature of the proton beam and a lateral displacement in AP direction of approximately 4 cm at iso-center. Consequently, the beam entrance in the

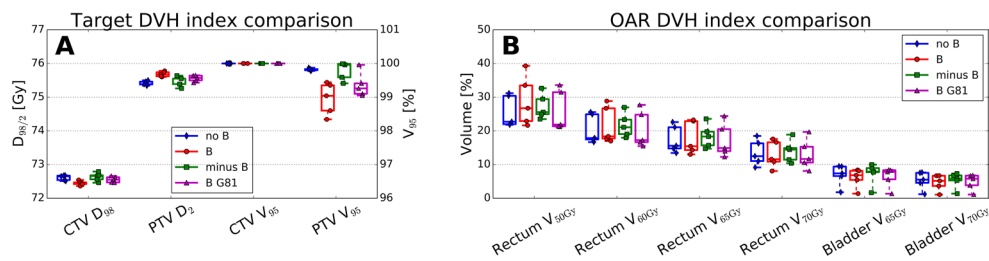


**Figure 2.** Dosimetric comparison of *no B*, *B*, *minus B* and *B G81* treatment plans optimized on *CT1*. Target (A) and OAR (B) DVH parameter data of all five patients were grouped using boxplots.

patient is shifted posteriorly for the *B* and anteriorly for the *minus B* scenario. At 81° gantry angle, beam deflection causes the beam to enter the patient almost horizontally and at a position similar to *no B*, as intended. It should be noted that for all *B*-field scenarios and patients, plans of comparable dosimetric quality to the *no B* reference could be obtained on *CT1* (see figure 2): CTV  $D_{98\%}$  and PTV  $D_{2\%}$  within 0.5 Gy, CTV  $V_{95\%}$  at 100%, as well as PTV  $V_{95\%}$  within 1.5% of the *no B* reference and above 98%. Dosimetric goals for the OARs could be fulfilled for every case. Rectum  $V_{60/65/70\text{ Gy}}$  and bladder  $V_{65/70\text{ Gy}}$  were within 4% of the *no B* scenario, with *minus B* plans showing a tendency of moderately increased rectum dose. For the *B* plans at 90° gantry angle, rectum  $V_{50\text{ Gy}}$  was increased by up to 8% because of the deflection and posterior displacement of the beam.

Looking at the dose recalculated on *CT2/3* of Pat1 in figure 1, a substantial overshoot of the proton beam was observed on *CT3* for the *B* scenario (see yellow circle) due to the posterior beam displacement and the more pronounced changes in the patient outline closer to the treatment table, as well as air cavities appearing in the rectum. Consequently, decrease of PTV coverage and rectal dose with respect to *CT1* was larger compared to the other three scenarios (see corresponding DVHs in figure 1).

Similar observations in terms of PTV coverage were made for most patients. Panels A and B of figure 3 illustrate the changes in all considered DVH parameters from *CT1* to *CT2/3* for *B*, *minus B* and *B G81* scenarios with respect to the changes observed for *no B*. Although, due to considerable anatomical changes from *CT1* to *CT2/3*, PTV  $V_{95\%}$ , CTV  $D_{98\%}$  and  $V_{95\%}$  were generally reduced on *CT2/3*, also for *no B*, the decrease in PTV  $V_{95\%}$  was significantly larger for *B* ( $p < 0.01$ ) and *B G81* ( $p = 0.04$ ) scenarios (figure 3(A)). Changing the gantry angle from 90° to 81°, however, clearly reduced differences with respect to *no B*: the maximum difference in PTV  $V_{95\%}$  decrease went from -9% to -3%, the median difference from -3.5% to -1.6%. With flipped magnetic field (*minus B*), PTV  $V_{95\%}$  decrease was similar to *no B*. All scenarios with *B*-field showed a significantly lower PTV  $D_{2\%}$  increase, with negligible absolute differences (<0.5 Gy) to *no B*. There were no statistically significant differences in the CTV DVH parameters. In terms of the OARs, anatomical changes introduced variations in rectum and bladder DVH parameter by up to 20% from *CT1* to *CT2/3* for all four considered scenarios. The only statistically significant differences compared to *no B* were a smaller increase of the bladder dose for *B* ( $p = 0.01$ , figure 3(B)), and a smaller rectum  $V_{50\text{ Gy}}$  increase for *B G81* ( $p = 0.01$ ), both at a negligible median difference of below 1%. Generally, changes in rectal DVH parameters on *CT2/3* were found closer to *no B* for a gantry angle of 81° compared to 90°. For *minus B*, rectum DVH parameter increased up to 7.5% stronger than for *no B* due to the beam curving from anterior to posterior, i.e. towards the rectum. The *B* scenario exhibited differences of up to -10% to *no B* due to proton overshoot caused by variations in rectum filling and the patient contour close to the treatment couch.

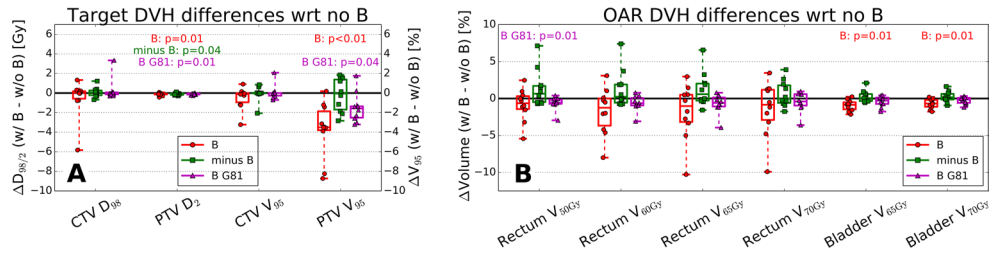


**Figure 3.** Boxplots of target (A) and OAR (B) DVH parameter changes on *CT2/3* compared to *CT1* for *B*, *minus B* and *B G81* scenarios. Data for all patients and repeated CTs are grouped using boxplots. All values are given with respect to the changes observed for *no B*. Statistically significant differences with respect to *no B* are indicated by the corresponding *p*-values.

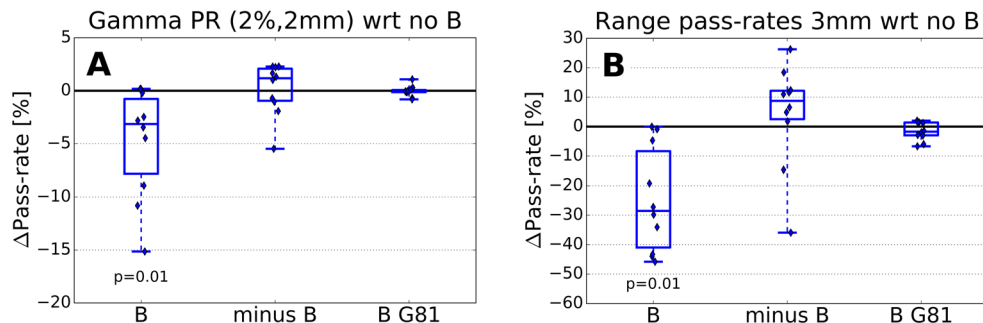


**Figure 4.** Boxplots of gamma-index (A) and range (B) pass-rate (PR) differences with respect to *no B*, comparing dose distributions on *CT1* to those on *CT2/3* for all patients. Statistically significant differences to *no B* are indicated by the corresponding *p*-values.

In line with these findings, range and gamma-test pass-rates were lowest for the *B* scenario when comparing dose calculations on *CT1* to those on *CT2/3* (figure 4). In particular, pass-rates were significantly reduced compared to the *no B* reference ( $p = 0.01$ ). For the *minus B* case, pass-rates were on average slightly higher than without *B*-field. For *B G81* pass-rates were most similar (within 7%) to *no B*, indicating a similar robustness against anatomical changes.

### 3.2. Robustness against positioning errors

Figure 5 illustrates the impact of  $\pm 5$  mm LR (panels (A)–(D)) and AP (panels (E)–(H)) shifts on the DVH curves of exemplary patient Pat3 for *no B*, *B*, *minus B* and *B G81* scenarios. With magnetic field, the dose distribution is no longer invariant under LR shifts, even if neglecting beam divergence. Compared to AP shifts, however, dosimetric variations were relatively small. Similar observations were made for all patients. Figures 6 and 7 illustrate the changes in all considered target and OAR DVH parameters under patient shifts for *B*, *minus B* and *B G81* in comparison to *no B*. For LR shifts, changes in CTV  $D_{98\%}$  and PTV  $D_{2\%}$  were mostly below 1 Gy, changes in CTV and PTV  $V_{95\%}$  below 1.5% for all B-field scenarios (figure 6(A)). Even though these changes are significantly different with respect to *no B*, which is invariant under LR shifts, they are deemed clinically not critical. In contrast, AP shifts led to a PTV  $V_{95\%}$  decrease by up to 15% on the shifted *CT1*. However, compared to

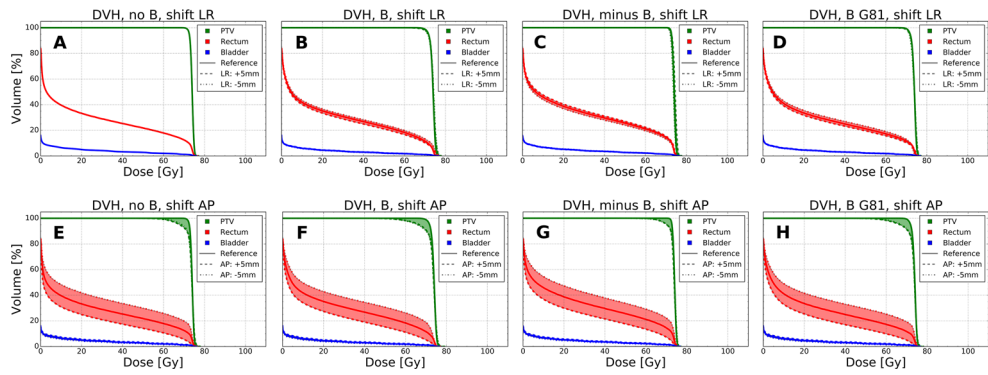


**Figure 5.** DVH band plots for LR ((A)–(D)) and AP ((E)–(H)) shifts of Pat3. *no B* ((A) and (E)), *B* ((B) and (F)), *minus B* ((C) and (G)) and *B G81* ((D) and (H)) scenarios are shown. The DVH bands correspond to  $\pm 5$  mm shifts in LR and AP direction, respectively.

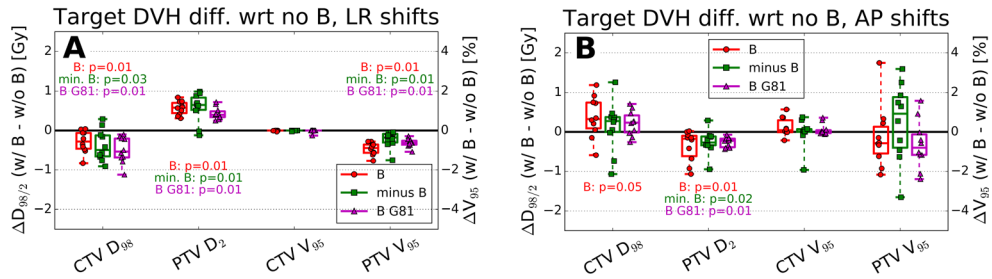


**Figure 6.** Boxplots of target DVH parameter changes for LR (A) and AP shifts (B) of CT1. All values are with respect to the changes observed for *no B*. Statistically significant differences to *no B* are indicated by the corresponding  $p$ -values.

*no B* (figure 6(B)), the impact of AP shifts was similar in the presence of a magnetic field. Changes in CTV  $D_{98\%}$  and PTV  $D_{2\%}$  were within 1.5% of the *no B* reference, changes in CTV and PTV  $V_{95\%}$  mostly within 3%. The only statistically significant differences to *no B* were a slightly higher CTV  $D_{98\%}$  for the *B* scenario, as well as a reduced PTV  $D_{2\%}$  for all scenarios with B-field under AP shifts. Also in terms of the OARs, AP shifts induced larger dosimetric changes, by up to  $\pm 15\%$ , in comparison to LR shifts, where changes were below  $\pm 4\%$ . Since the effects of left and right shifts on the OAR DVH parameters are opposite (increase and decrease or vice versa), there is no net effect expected from a random LR shift in presence of a magnetic field (figure 7(A)). Also for AP shifts, no significant differences with respect to *no B* were found for any scenario with B-field. OAR DVH parameter changes were mostly within 2% (figure 7(B)). No considerable differences in terms of the robustness against positioning errors were indicated between *B*, *minus B* and *B G81*, neither in terms of target nor in terms of OAR DVH parameters.

#### 4. Discussion

Dosimetrically comparable PBS-PT plans could be generated using inverse planning on segmented CT images for five prostate cancer patients, considering four different scenarios (*no B*, *B*, *minus B*, *B G81*). Dose re-calculations on repeated CT images showed a clearly reduced

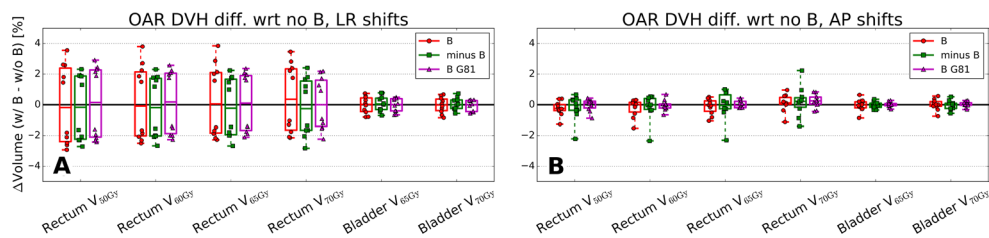


**Figure 7.** Boxplots of OAR DVH parameter changes for LR (A) and AP shifts (B) of CT1. All values are with respect to the changes observed for *no B*.

robustness against anatomical changes in the presence of a +1.5 T B-field at 90° gantry angle (*B*) with respect to *no B*. Gamma-index pass-rates and proton range agreement were significantly lower. Moreover, a significantly stronger decrease of PTV  $V_{95\%}$  was found. CTV dosimetric parameters were mostly not affected by the magnetic field for the used 10 mm CTV to PTV margin. If applying tighter margins, as potentially intended by improved MR-based image-guidance, CTV coverage might become affected in a similar way. The reduced robustness could be attributed to more pronounced changes in the patient outline closer to the treatment table (Maspero *et al* 2017), as well as to an increased sensitivity to changes in the rectum air cavities being traversed by an increased number of pencil-beams with respect to *no B*. The slightly longer beam path within the patient might further diminish robustness.

By either flipping the orientation of the magnetic field (*minus B*) or changing the gantry angle to 81° (*B G81*) in order to correct for the beam deflection and lateral displacement, robustness against anatomical changes could straightforwardly be improved. Instead of flipping the magnetic field, the patient position might be changed from ‘head-first’ to ‘feet-first’ in clinical practice or the gantry rotated to an angle of 270°. While the *minus B* scenario still showed a slight tendency of stronger rectal dose increase, probably due to the beam bending towards the rectum, the *B G81* scenario was found similar to the *no B* reference in all investigated aspects. The only noticeable difference was a larger PTV  $V_{95\%}$  reduction attributed to the curvature of the beam close to the PTV, making it slightly more sensitive to changes in the rectum air cavities. Since the median decrease is only 1.6% larger than for *no B*, an equal robustness against anatomical changes for *B G81* and *no B* might be concluded from a dosimetric point of view. In particular, no implications due to the electron-return-effect were observed because of the comparably low energy of secondary electrons in proton radiotherapy (Raaymakers *et al* 2008).

In the presence of magnetic fields the dose distribution is no longer invariant under LR shifts at 90° gantry angle. Dosimetric changes were, however, only minor and clearly smaller than for AP shifts. With respect to *no B*, in particular, no relevant differences were found for any scenario with B-field for LR and AP shifts, indicating no considerable impact of the magnetic field on the robustness against positioning errors. Given the uniformity and infinite length of the modelled B-field in SI direction, only a minor impact of the B-field is anticipated for SI shifts, as well. In particular, the position of the patient with respect to the magnetic field will not change when introducing ±5 mm SI shifts. Changes in the considered DVH parameters will thus be governed by geometrical considerations which are similar with and without magnetic field. This would also hold true in a more realistic MRI B-field, which is approximately constant along the scanner axis in the center of the field-of-view.

Based on the results of our study, which suggest that an equivalent robustness of PBS-PT with and without magnetic field can be attained, it may be concluded that PBS-PT for prostate cancer could benefit from MRI-guidance even before dedicated pre-treatment adaptation

strategies become clinically available. In particular, the enhanced soft-tissue contrast of *in situ* MRI could be exploited for improved, marker-free target visualization, more accurate patient positioning and margin reduction to foster image-guided PT. Also when pre-treatment PBS-PT plan adaptation becomes available in the future, a more robust beam set-up as introduced in this work would be clinically preferable in view of fast intra-fractional changes, such as rectum filling, which would otherwise require highly advanced real-time adaptation strategies.

The results of this study are based on a comparably small number of representative patients for the specific indication of prostate cancer. Strategies for improving the robustness of PBS-PT in the presence of magnetic fields might be different for other treatment sites. In particular, the differences observed in the robustness of *B* and *minus B* scenarios are attributed to the specific anatomical conditions of prostate cancer, where anatomical changes (rectal filling, outer contour) are more pronounced posteriorly of the PTV, such that due to deflection and lateral displacement of the proton beam the *B* scenario is substantially stronger affected. A simple iso-center shift (corresponding to the *B* scenario), might thus result in clinically satisfying dose distributions on the nominal planning CT, as first shown also by Moteabbed *et al* (2014) for two prostate cases using passively delivered proton beams, but might not be the optimal choice in terms of treatment robustness. Speaking more generally, also for treatment sites other than the prostate, scenarios where curvature and lateral deflection of the proton beam cause it to pass regions of pronounced anatomical changes should be avoided for the sake of treatment robustness. The alternative strategy studied in this work for enhancing robustness of PBS-PT in an MRI *B*-field by beam angle correction in combination with an iso-center shift, aiming in particular at reproducing similar proton trajectories from entrance to target volume in the patient as observed without magnetic field (corresponding to the *B G81* scenario), is expected to be a more general recipe that is potentially also applicable to other treatment sites. Even for the considered deep-seated prostate target volumes and a 1.5 T magnetic field, differences in beam path between *B G81* and *no B* due to curvature of the proton beam were only minor within the patient and consequently robustness with and without magnetic field similar. This finding might also be taken into account in the development of methods for correcting the proton beam deflection in magnetic fields (Schellhammer and Hoffmann 2017), which might benefit from considering treatment robustness by aiming at finding iso-center shifts and gantry angle corrections that minimize differences in proton beam trajectories with and without *B*-field. Such corrections will eventually depend on the strength of the magnetic field, its specific shape, as well as the anatomical conditions of the treated site, and herewith the used proton energies, but enable to directly translate the most robust gantry angles used in today's clinical PT practice to MRI-guided PBS-PT. The exact iso-center shift and gantry angle correction for a specific scenario, which we obtained following careful investigation of a range of potential gantry angles, might in the future also be determined by estimating the lateral displacement and resulting deflection angle of an average energy pencil-beam, following, e.g. the approach outlined by Hartman *et al* (2015).

It should also be noted that a simplified homogeneous and spatially confined magnetic field was assumed in this contribution. MRI fringe fields might slightly alter the beam path and affect the robustness against anatomical changes and positioning errors of different gantry angles. Further technical options, beyond the scope of this study, for improving the robustness of MRI-guided PBS-PT could be imaging at lower field strength, e.g. at ~0.3 T, and hereby minimizing the deflection of the proton beams, or aligning the proton beam and magnetic field in order to avoid lateral deflection of the initial beam. A detailed investigation on potential beam line and MRI-guided PT treatment machine designs can be found in Oborn *et al* (2015, 2017).

Another subject beyond the scope of this contribution that should be carefully addressed in the context of MRI-guided PT is the effect of magnetic fields on clinical proton dosimetry, e.g. for beam calibration, monitoring and quality assurance, as well as for monitor unit calculation. Due to differences in the secondary electron spectrum it is, in particular, not *a priori* clear whether concepts currently developed for dosimetry in MRI-guided photon therapy can be straightforwardly translated to MRI-guided PT (Oborn *et al* 2017). In line with this, it is also desirable to perform a thorough experimental validation of the MC dose calculations in terms of their dosimetric accuracy by comparison to measurements in the future. This, however, requires a magnet generating a realistic MRI-like B-field and a proton PBS system, the combination of which is currently not accessible to our group.

## 5. Conclusions

The results obtained in this study indicate that robustness of PBS-PT for prostate cancer against positioning errors is not diminished by the presence of a magnetic field. Robustness against anatomical changes, on the other hand, was found to be clearly affected by the B-field and to depend on the orientation of the patient with respect to the magnetic field, as well as on the gantry angle. For the investigated prostate cancer patient cohort, robustness was substantially reduced for the *B* scenario with respect to *no B*, but could be improved considerably by inverting the magnetic field (*minus B*) or by adapting the gantry angle (*B G8I*). Results suggest that MRI-guided PT might achieve robustness similar to current CT-guided PT without B-field, also for treatment sites other than the prostate, if the treatment parameters are adapted such that differences between the proton trajectories with and without magnetic field are minimized within the patient.

## Acknowledgments

This work was supported by the German Cancer Aid (Deutsche Krebshilfe) and the German Research Foundation (DFG) Cluster of Excellence Munich-Centre for Advanced Photonics (MAP). Fruitful discussions with Daniel Köpl and Martin Hillbrand on treatment planning are gratefully acknowledged. Prof J Wilkens is acknowledged for sharing the research proton TPS. Prof F Verhaegen and Dr M Podesta are acknowledged for sharing the gamma-evaluation software used in this study.

## References

- Acharya S *et al* 2016 Online magnetic resonance image guided adaptive radiation therapy: first clinical applications *Int. J. Radiat. Oncol. Biol. Phys.* **94** 394–403
- Agostinelli S *et al* 2003 GEANT4-a simulation toolkit *Nucl. Instrum. Methods Phys. Res. A* **506** 250–303
- Beltran C, Herman M G and Davis B J 2008 Planning target margin calculations for prostate radiotherapy based on intrafraction and interfraction motion using four localization methods *Int. J. Radiat. Oncol. Biol. Phys.* **70** 289–95
- Deasy J O, Blanco A I and Clark V H 2003 CERR: a computational environment for radiotherapy research *Med. Phys.* **30** 979–85
- Durante M and Loeffler J S 2010 Charged particles in radiation oncology *Nat. Rev. Clin. Oncol.* **7** 37–43
- Engelsman M, Schwarz M and Dong L 2013 Physics controversies in proton therapy *Semin. Radiat. Oncol.* **23** 88–96
- Fallone B G 2014 The rotating biplanar linac-magnetic resonance imaging system *Semin. Radiat. Oncol.* **24** 200–2

- Fuchs H, Moser P, Groschl M and Georg D 2017 Magnetic field effects on particle beams and their implications for dose calculation in MR guided particle therapy *Med. Phys.* **44** 1149–56
- Glitzner M, Crijns S P, de Senneville B D, Kontaxis C, Prins F M, Lagendijk J J and Raaymakers B W 2015 On-line MR imaging for dose validation of abdominal radiotherapy *Phys. Med. Biol.* **60** 8869–83
- Hartman J, Kontaxis C, Bol G H, Frank S J, Lagendijk J J, van Vulpen M and Raaymakers B W 2015 Dosimetric feasibility of intensity modulated proton therapy in a transverse magnetic field of 1.5 T *Phys. Med. Biol.* **60** 5955–69
- Jaffray D A 2012 Image-guided radiotherapy: from current concept to future perspectives *Nat. Rev. Clin. Oncol.* **9** 688–99
- Keall P J, Barton M and Crozier S 2014 The Australian magnetic resonance imaging-linac program *Semin. Radiat. Oncol.* **24** 203–6
- Kontaxis C, Bol G H, Lagendijk J J and Raaymakers B W 2015 A new methodology for inter- and intrafraction plan adaptation for the MR-linac *Phys. Med. Biol.* **60** 7485–97
- Kotte A N, Hofman P, Lagendijk J J, van Vulpen M and van der Heide U A 2007 Intrafraction motion of the prostate during external-beam radiation therapy: analysis of 427 patients with implanted fiducial markers *Int. J. Radiat. Oncol. Biol. Phys.* **69** 419–25
- Kurz C, Dedes G, Resch A, Reiner M, Ganswindt U, Nijhuis R, Thieke C, Belka C, Parodi K and Landry G 2015 Comparing cone-beam CT intensity correction methods for dose recalculation in adaptive intensity-modulated photon and proton therapy for head and neck cancer *Acta Oncol.* **54** 1651–7
- Kurz C et al 2016 Investigating deformable image registration and scatter correction for CBCT-based dose calculation in adaptive IMPT *Med. Phys.* **43** 5635
- Lagendijk J J, Raaymakers B W, Van den Berg C A, Moerland M A, Philippens M E and van Vulpen M 2014a MR guidance in radiotherapy *Phys. Med. Biol.* **59** R349–69
- Lagendijk J J, Raaymakers B W and van Vulpen M 2014b The magnetic resonance imaging-linac system *Semin. Radiat. Oncol.* **24** 207–9
- Lutgendorf-Caucig C, Fotina I, Stock M, Potter R, Goldner G and Georg D 2011 Feasibility of CBCT-based target and normal structure delineation in prostate cancer radiotherapy: multi-observer and image multi-modality study *Radiother. Oncol.* **98** 154–61
- Marks L B, Yorke E D, Jackson A, Ten Haken R K, Constine L S, Eisbruch A, Bentzen S M, Nam J and Deasy J O 2010 Use of normal tissue complication probability models in the clinic *Int. J. Radiat. Oncol. Biol. Phys.* **76** S10–9
- Maspero M, Seevinck P R, Schubert G, Hoesl M A, van Asselen B, Viergever M A, Lagendijk J J, Meijer G J and van den Berg C A 2017 Quantification of confounding factors in MRI-based dose calculations as applied to prostate IMRT *Phys. Med. Biol.* **62** 948–65
- Mendenhall N P, Hoppe B S, Nichols R C, Mendenhall W M, Morris C G, Li Z, Su Z, Williams C R, Costa J and Henderson R H 2014 Five-year outcomes from 3 prospective trials of image-guided proton therapy for prostate cancer *Int. J. Radiat. Oncol. Biol. Phys.* **88** 596–602
- Moteabbed M, Schuemann J and Paganetti H 2014 Dosimetric feasibility of real-time MRI-guided proton therapy *Med. Phys.* **41** 111713
- Mutic S and Dempsey J F 2014 The ViewRay system: magnetic resonance-guided and controlled radiotherapy *Semin. Radiat. Oncol.* **24** 196–9
- Noel C E, Parikh P J, Spencer C R, Green O L, Hu Y, Mutic S and Olsen J R 2015 Comparison of onboard low-field magnetic resonance imaging versus onboard computed tomography for anatomy visualization in radiotherapy *Acta Oncol.* **54** 1474–82
- Oborn B M, Dowdell S, Metcalfe P E, Crozier S, Mohan R and Keall P J 2015 Proton beam deflection in MRI fields: implications for MRI-guided proton therapy *Med. Phys.* **42** 2113–24
- Oborn B M, Dowdell S, Metcalfe P E, Crozier S, Mohan R and Keall P J 2017 Future of medical physics: real-time MRI-guided proton therapy *Med. Phys.* **44** e77–90
- Padhani A R, Khoo V S, Suckling J, Husband J E, Leach M O and Dearnaley D P 1999 Evaluating the effect of rectal distension and rectal movement on prostate gland position using cine MRI *Int. J. Radiat. Oncol. Biol. Phys.* **44** 525–33
- Paganetti H 2012 Range uncertainties in proton therapy and the role of Monte Carlo simulations *Phys. Med. Biol.* **57** R99–117
- Parodi K, Mairani A, Brons S, Hasch B G, Sommerer F, Naumann J, Jakel O, Haberer T and Debus J 2012 Monte Carlo simulations to support start-up and treatment planning of scanned proton and carbon ion therapy at a synchrotron-based facility *Phys. Med. Biol.* **57** 3759–84

- Raaymakers B W, Raaijmakers A J and Lagendijk J J 2008 Feasibility of MRI guided proton therapy: magnetic field dose effects *Phys. Med. Biol.* **53** 5615–22
- Rasch C, Barillot I, Remeijer P, Touw A, van Herk M and Lebesque J V 1999 Definition of the prostate in CT and MRI: a multi-observer study *Int. J. Radiat. Oncol. Biol. Phys.* **43** 57–66
- Resch A F, Landry G, Kamp F, Cabal G, Belka C, Wilkens J J, Parodi K and Dedes G 2017 Quantification of the uncertainties of a biological model and their impact on variable RBE proton treatment plan optimization *Phys. Med.* **36** 91–102
- Rit S, Clackdoyle R, Keuschnigg P and Steininger P 2016 Filtered-backprojection reconstruction for a cone-beam computed tomography scanner with independent source and detector rotations *Med. Phys.* **43** 2344
- Schell S and Wilkens J J 2010 Advanced treatment planning methods for efficient radiation therapy with laser accelerated proton and ion beams *Med. Phys.* **37** 5330–40
- Schellhammer S M and Hoffmann A L 2017 Prediction and compensation of magnetic beam deflection in MR-integrated proton therapy: a method optimized regarding accuracy, versatility and speed *Phys. Med. Biol.* **62** 1548–64
- Schneider W, Bortfeld T and Schlegel W 2000 Correlation between CT numbers and tissue parameters needed for Monte Carlo simulations of clinical dose distributions *Phys. Med. Biol.* **45** 459–78
- Stuetzer K, Paessler T, Valentini C, Exner F, Thiele J, Hoelscher T, Krause M and Richter C 2016 SU-F-J-203: retrospective assessment of delivered proton dose in prostate cancer patients based on daily in-room CT imaging *Med. Phys.* **43** 3455
- Trofimov A, Nguyen P L, Coen J J, Doppke K P, Schneider R J, Adams J A, Bortfeld T R, Zietman A L, Delaney T F and Shipley W U 2007 Radiotherapy treatment of early-stage prostate cancer with IMRT and protons: a treatment planning comparison *Int. J. Radiat. Oncol. Biol. Phys.* **69** 444–53
- Trofimov A, Nguyen P L, Efsthathiou J A, Wang Y, Lu H M, Engelsman M, Merrick S, Cheng C W, Wong J R and Zietman A L 2011 Interfractional variations in the setup of pelvic bony anatomy and soft tissue, and their implications on the delivery of proton therapy for localized prostate cancer *Int. J. Radiat. Oncol. Biol. Phys.* **80** 928–37
- Veiga C et al 2016 First clinical investigation of cone beam computed tomography and deformable registration for adaptive proton therapy for lung cancer *Int. J. Radiat. Oncol. Biol. Phys.* **95** 549–59
- Villeirs G M, Van Vaerenbergh K, Vakaet L, Bral S, Claus F, De Neve W J, Verstraete K L and De Meerleer G O 2005 Interobserver delineation variation using CT versus combined CT + MRI in intensity-modulated radiotherapy for prostate cancer *Strahlenther. Onkol.* **181** 424–30
- Wolf R and Bortfeld T 2012 An analytical solution to proton Bragg peak deflection in a magnetic field *Phys. Med. Biol.* **57** N329–37